Cancer Nanotechnology

RESEARCH

Open Access

Nickel-gallate metal–organic framework as an efficient antimicrobial and anticancer agent: in vitro study

Ahmed. A. G. El-Shahawy[1], Esam M. Dief[1*], S. I. El-Dek[1], A. A. Farghali[1] and Fatma I. Abo El-Ela[2*]

*Correspondence: essam.dief@gmail.com; fatma.aboelela@vet.bsu.edu.eg; fa.pharma@yahoo.com

[1] Materials Science and Nanotechnology Department, Faculty of Postgraduate Studies for Advanced Sciences (PSAS), Beni-Suef University, Beni-Suef, Egypt

[2] Pharmacology Department, Faculty of Veterinary Medicine, Beni-Suef University, Beni-Suef 62511, Egypt

Abstract

Gallic acid is a natural antioxidant present in many plants such as tea, sumac, gallnut and other plants. This naturally occurring gallic acid is known to exhibit auto-oxidation under certain conditions, generating several reactive oxygen species (ROS) including superoxides, hydroxyls and hydrogen peroxide radicals that plays key roles in its antimicrobial activity. Here, we demonstrate that incorporating gallic acid as a linker in Ni-based metal organic frameworks (Ni-gallate MOFs) produces mesoporous nanostructures with antimicrobial and anticancer activity. The synthesized Ni-gallate MOFs have shown antibacterial activity against both Gram-positive and Gram-negative bacteria, and antifungal activity against two different strains of fungi species. Furthermore, Ni-gallate MOFs have shown a significant cytotoxic effect on rhabdomyosarcoma (RMS) cells, compared to the standard anticancer drug, Doxorubicin. In this study, the Ni-gallate MOF nanostructures were characterized using scanning electron microscope (SEM), energy dispersive X-ray (EDX), X-ray diffraction (XRD), Fourier transform infra-red (FTIR), and Brunauer–Emmett–Teller (BET) method for surface area. The antibacterial and antifungal activity of gallic acid-based mesoporous framework nanostructure were tested, suggesting that Ni-gallate MOF has a dual anticancer and antimicrobial activity.

Keywords: Antimicrobial, Antitumor, Gallic acid, Metal organic frameworks

Introduction

Metal organic frameworks (MOFs) have emerged as a new and a remarkable class of crystalline porous materials that form one, two and three-dimensional structures (Yaghi et al. 2003). Due to their high porosity and capacity; MOFs have been widely used in gas storage applications (Furukawa et al. 2013). In addition, the facile synthesis and functions of MOFs have opened new venues for these coordination polymers in many biological applications (Czaja et al. 2009; Tanabe and Cohen 2011) such as bio-sensing (Chen et al. 2010; Kumar et al. 2015; Ren et al. 2013) bio-imaging (DF et al. 2017; McKinlay et al. 2010) and controlled release of drugs other bioactive molecules (McKinlay et al. 2010; Horcajada et al. 2010; Kitagawa et al. 2004; Liu et al. 2014). Recently, MOFs have been utilized as drug delivery platforms and antibacterial agents (Kaur et al. 2020; Lawson

et al. 2021; Wu and Yang 2017; Eckshtain-Levi et al. 2022; Maranescu and Visa 2022; Yan et al. 2022).

Compared to inorganic microporous zeolites, MOFs have shown several outstanding properties, in particular, large surface area with high compositional tunability, which can be achieved by using different metals or changing the organic linker (Badhani et al. 2015; Dorman et al. 2011) .

It is important to realize that gallic acid linker has been utilized to prepare isostructural transition metal gallate dehydrates with high crystallinity and reproducibility (Wang et al. 2017). Gallic acid (GA) is an organic polyhydroxyphenolic compound (3,4,5-trihydroxybenzoic acid, $C_7O_5H_6$) that able to form chelates with transition metal ions due to presence of large gaps between five available oxygen atoms that distributed on opposite sides of the phenyl rings. Besides, GA has been demonstrated to endure autoxidation in specific conditions and to exhibit a pro-oxidant activity (Sourani et al. 2016; Wyszogrodzka et al. 2016). The pro-oxidant potential of GA results in generation of several reactive oxygen species (ROS) including superoxides, hydroxyls and hydrogen peroxide radicals; these free radicals has been considered as the key factor of its antimicrobial activity (Feller and Cheetham 2006; Ponce et al. 2016). Recently, magnesium and iron gallate MOFs structures have been reported to exploit high antibacterial activities (Cooper et al. 2015). In addition, GA has been widely incorporated with nanostructures to enhance their anticancer efficiency (Cooper et al. 2015; Boer et al. 2014).

Indeed, the axial head and neck rhabdomyosarcoma (HRMS) is an aggressive soft tissue tumor in children. All children with HRMS are treated either by surgery, chemotherapy and radiation therapy or a combination between them. It is evidenced that all of these treatments have limitations and side effects (Zhou et al. 2015). On the other hand, Gram-positive (*St. coccus, S. aureus*) and Gram-negative *(E. coli and P. Aeruginosa)* are microbial agents of multiple infective diseases in humans. The emergence of antibiotic-resistant strains of *S. aureus* such as methicillin-resistant *S. aureus* is a worldwide problem in clinical medicine (Chambers and DeLeo 2009). Despite of developing researches, there is no approved vaccine for *S. aureus* and *St. coccus*. Also, antibiotic resistance of *E. coli* strains is consistently rising, especially resistance to important antibiotics as Cephalosporin and Fluoroquinolones (Park 2014).

Due to the fact that GA is naturally present in several kinds of fruits and vegetables, and nickel is a stable transition metal that takes part in many biological processes. In addition, the effect of Ni-gallate-MOF on RMS has not been investigated. The current study has harnessed the potential of MOF constructed from GA linker with nickel metal. Here, we investigate the prepared antibacterial, antifungal and anticancer activity of the as-synthesized Ni-gallate-MOF, compared to standard antibiotics, antifungal and anticancer drugs.

Materials and methods

Materials

N,*N*-Dimethylformamide (DMF), gallic acid monohydrate 98% were bought from Sigma-Aldrich (UK). Methanol 99.9% was purchased from CARLO ERBA Reagents, France. All reagents used in this work were of analytical grade. HNRMS cell lines were obtained from the American Type Culture Collection (ATCC, Rockville, MD, USA). Dimethyl

sulfoxide (DMSO), MTT and trypan blue dyes were purchased from Sigma (St. Louis, MO, USA). Fetal Bovine serum, DMEM, RPMI-1640, HEPES buffer solution, L-glutamine, gentamycin and 0.25% Trypsin-EDTA were procured from Lonza (Belgium). Doxorubicin as a reference standard was taken from Sigma Aldrich. For antibacterial study, Gram-positive *St. coccus* (ATCC 49619), *S. aureus* (ATCC 25913), Gram-negative *E. coli* (ATCC 25922) and *P. Aeruginosa* (ATCC 27853), as well, two different strains of fungi species (*Aspergillus flocculosus* and *Aspergillus nigricans*) were purchased from Cairo Microbiology Research Center. Muller–Hinton broth was used to culture *E. coli*, *S. aureus*, *St. coccus* and *P. aeruginosa* at 37 °C for 24 h in an incubator. All tubes were sterilized in an autoclave before the experiments.

Synthesis of Ni-gallate MOF

Ni-gallate MOF was prepared with the slightly modified solvothermal method (Jiao et al. 2017). Briefly, under continuous magnetic stirring for 30 min, a solution of nickel nitrate—$NiNO_3.6H_2O$, 4 mmol (1.16 g) + 15.6 ml DMFDMF—was added drop-wise to a sol of GA (GA monohydrate, 2 mmol (0.39 g) + 10 ml DMF). Thereafter, the mixture was heated in 80 ml Teflon-lined stainless-steel autoclave at 120 °C for 16 h, and it was cooled at room temperature. After a few hours, a brown precipitate was collected, separated via centrifugation for 5 min at 6000 rpm and washed 2 times with DMF. Finally, the precipitate was subjected to solvent exchange with methanol 6 times over 3 days and was dried in a vacuum oven at 100 °C for 12 h. It's noteworthy to mention that solvent exchange step aims at activating the framework structure by replacing DMF with a low boiling point solvent, methanol, and thus assists in solvent removal from the pores at relatively lower temperatures.

Material characterization

A profile FTIR spectrum of Ni-Gallate MOF was obtained using FTIR spectrometer (Shimadzu) with a range of 800 4000 cm^{-1}. The samples were prepared as KBr pellet and were scanned against a KBr pellet background. The crystallinity of Ni-gallate MOF was investigated by X-ray diffractometer (ANalytical Empyrean, The Netherlands) with CuKα radiation (40 kV, current 35 mA), scanning range 10–70°, scan step 0:05° and wavelength λ = 1.54045 Å. The (BET) surface area, pore size, pore volume distribution, as well as the N_2 adsorption/desorption isotherms were measured using surface area analyzer (TriStar II 3020, Micromeritics, USA). Field emission scanning electron microscopy (FESEM) images of Ni-gallate MOF were acquired using a Quanta FEG 250 (Switzerland). The EDX for qualitative and quantitative analysis was performed at the same instrument.

Anticancer measurements

Viable cells counting (trypan blue assay)

The treated RMS cells with Ni-Gallate MOF were separated using 0.25% trypsin for 10 min; 10 µl of the cell suspension were combined with 10 µl of trypan blue solution: 0.4% prepared in 0.81% sodium chloride and 0.06% dibasic potassium phosphate. The mixture was incubated at room temperature for 5 min, and 10 µl of the mixture were

counted by the traditional cell counting; the percentage of the unstained cells represents that of viable cells in the suspension (Gomha et al. 2015):

$$\%\text{viable cells} = (\text{number of viable cells/Number of total cells}) \times 100.$$

Antitumor activity MTT assay

The RMS cells were suspended in a RPMI-1640 medium that supplemented with 10% in-activated fetal calf serum and 50 µg/ml gentamycin; the cells were maintained at 37 °C in a humidified atmosphere with 5% CO_2 and sub-cultured three times a week. For the cytotoxicity evaluation, the cell viability and inhibitory percent were determined by MTT assay.

Briefly, the suspended RMS cells were placed in Corning® 96-well tissue culture plate with a concentration 5×10^4 cell/well; it was incubated for 24 h. Thereafter, serial two-fold dilutions of the tested Ni-gallate MOF were added to the RMS cells that incubated again for 24 h. Then, the medium was removed from each well and substituted with 100 µl of fresh culture RPMI 1640 medium; 10 µl of the 12 mM MTT stock solution (5 mg of MTT in 1 mL of PBS) was annexed into each well and the treated RMS cells were incubated for 4 h. Finally, from each well, 85 µl of the medium were replaced by 50 µl of DMSO and the treated RMS cells were incubated for 10 min. The cell viability and inhibitory percentage were measured according to Bernas and Dobrucki (2002). The experiments and measurements were conducted three times; the results were reported as the average ± standard deviation.

The relation between tested Ni-gallate MOF against inhibitory and viability percent was plotted in a bar chart using Origin 8 software; the 50% inhibitory concentration (IC_{50}), which is the concentration required to cause toxic effects in 50% of intact cells was determined. In addition, the efficacy of the tested Ni-gallate MOF was compared with a standard doxorubicin.

Morphological analysis

The studied RMS cells at the same serial twofold dilutions of the tested Ni-gallate MOF, as well as, the control cells, were incubated at 37 °C for 24 h. Subsequently, the cells were scrubbed three times with 100 µl of phosphate-buffered saline (PH 7.2), fixed with 10% formalin for 15 min at room temperature and stained with 100 µl of 0.25% crystal violet for 20 min. Then, the stain was removed, and the cells were rinsed using deionized water to remove the excess of stain and allowed to dry. The cellular morphology was studied using an inverted microscope (CKX41; Olympus, Japan) equipped with the digital microscopy camera to catch the images describing the morphological variations that compared with control cells.

Antimicrobial measurements

To estimate the effectiveness of Ni-gallate MOF as antimicrobial agent, Gram-positive (*St. coccus, S. aureus*) and Gram-negative (*E. coli and P. aeruginosa*) were chosen for this investigation. *E. coli* (ATCC 25922), *S. aureus* (ATCC 25913), *St. coccus* (ATCC 49619), and *P. aeruginosa* (ATCC 27853), as well as, two different strains of fungi species (*Aspergillus flocculosus* and *Aspergillus nigricans*), were purchased from Cairo Microbiology

Research Center. In addition, the efficiency of Ni-gallate MOF was compared to standard antibiotic; tylvalosin for Gram-positive and Draxxin for Gram-negative that were obtained in a pure form from *Pharma Swede Pharmaceutical Company*.

The antimicrobial competence of Ni-gallate MOF versus the forementioned pathogens was determined by measuring the inhibition zone diameter utilizing agar dilution method. In respect of this point, a quantity of 100µL of each pathogen was aseptically spread on the surface of a separate Muller–Hinton agar plate using sterile bench Hockey stick; each plate was left on the bench for thirty minutes to pre-diffuse into the medium. Next, sterile discs that impregnated over-night in twofold serial dilutions of Ni-gallate MOF (1000, 250, 125 and 62.5 µg/ml) were stacked on each plate using a sterile Cork Borer set of 5 mm. It is important to bear in mind, the standard antibiotics, which mentioned above were strapped for comparison. Finally, all plates were incubated at 37 °C for 48 h.

It should be noted that the minimum inhibitory concentration (MIC) of the tested Ni-gallate MOF versus the aforesaid microbes was determined employing micro-dilution test. In accordance with this method, a stock solution of Ni-gallate MOF was prepared, and serially diluted into multiple sterilized tubes containing 10^8 CFU/ml of the tested bacteria that inoculated with Mueller–Hinton Broth medium, which was favored; due to its ability to support the growth of most pathogens and its lack of inhibitors towards common antibiotics. All tubes were incubated at 37 °C for 24 h. For verification, a tube of positive control—broth without tested pathogen and another one of negative control Broth with the tested microorganism was included. It is worth noting that by evaluation the turbidity of the examined tubes, the MIC was determined as the lowest concentration that had no visible turbidity and matched with positive control. With respect to minimal bactericidal concentration (MBC) measurement, the dilution representing the MIC and at least two of the more concentrated tested Ni-gallate MOF dilutions are plated on Muller–Hinton agar plate and enumerated to determine viable CFU/ml. After incubation at 37 °C for 24 h, the MBC is the lowest concentration that demonstrates a pre-determined reduction (such as 99.9%) in CFU/ml when compared to the MIC dilution; in the sense that MBC is the lowest concentration of the Ni-gallate MOF in which no viable bacterial colonies are observed (bactericidal activity).

Results and discussion

Material characterization

Figure 1 displays the X-ray diffraction pattern of GA and Ni-gallate MOF. The gallic acid reflected its nature crystallinity revealing sharp and intense diffraction peaks at diffraction angles. It is important to note that due to the presence of three phenolic OH groups and one carboxylic OH in the structure of gallic acid linker; its chelation with transition metal ions (M) has been reported to be dependent on the pH of the reaction media. Hence, previous studies have reported that two different phases of the crystal structure can be formed; the first is a protonated phase at pH 7–8, with two water molecules present in a structure of (M (H2gal).2H_2O). While the second phase ~ pH 12; it is a deprotonated form (M2 (gal). xH_2O) with unknown number of water molecules that embedded in the crystal lattice (Chambers and DeLeo 2009). Herein, the deprotonated

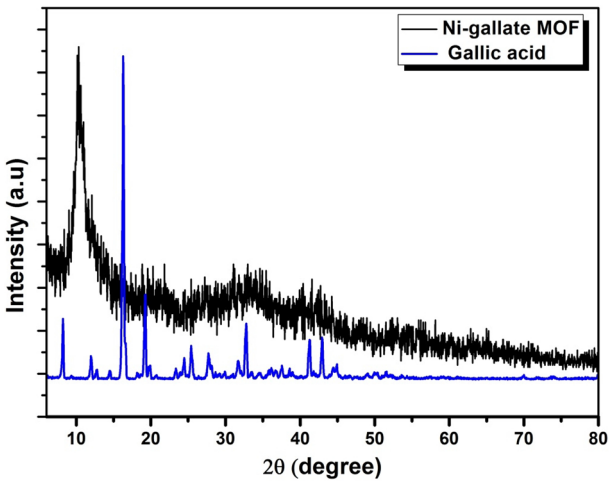

Fig. 1 Powder XRD pattern for Gallic acid powder (blue) and Ni-Gallate MOF (black)

form of Ni-gallate MOFs was synthesized; it was not possible to characterize the structure because of its poor crystallinity. This was obviously clear from the XRD spectrum.

The XRD pattern of Ni-gallate MOF revealed vanishing of large diffraction peaks of GA indicating the chelation of nickel atoms with gallic acid to form Ni-gallate MOF structures. Further, Ni-gallate MOF exhibited a broad single diffraction peak at 10.57°, which may be due to the poor crystalline nature of the MOF. As a result, the gallic acid is no longer present as a perfect ordered material, and its nickel complex existed in an amorphous state. The obtained PXRD pattern of Ni-gallate MOF is in consistence with a previously reported Mg-gallate structure (Zhao et al. 2016), as well as, the XRD pattern of Cu-gallate composites (Masoud et al. 2012).

The possible interaction between GA and Ni was studied by IR spectroscopy. Figure 2 illustrates the FTIR spectrum of GA and Ni-gallate MOF. In agreement with (Mu et al. 2017), gallic acid spectrum revealed two characteristic bands of carboxylic acid. The first is a strong broad band assigned to υ (O–H) stretching of carboxylic group at 3600−2500 cm^{-1}, while the second is a feeble υ (C=O) stretching at 1570 cm^{-1}, which disappeared in Ni-gallate MOF; suggesting that the coordination between gallic acid and Ni element affected the carbonyl group (Lu et al. 2016).

In contrast, the FTIR spectrum of Ni-GA MOF structure is completely different; it displays characteristic bands of GA linker at 1590 and 1386 cm^{-1}. These are due to asymmetry and symmetry stretching modes υ (COO^{-}), respectively. It is obvious that the intensity of transmitted band of asymmetric stretching mode is high comparing to symmetric one, in a total agreement with (Borges et al. 2013). In addition, these two bands were split, implying that GA is coordinated with nickel via a polydentate ligand mode.

Further, the wide stretching υ (O–H) band at 3383 cm^{-1} asserts the presence of water molecules in the Ni-GA MOF structure, another υ (O–H) of phenolic group at 2927 cm^{-1}. The band located at 1067 cm^{-1} is assigned to the C–H stretching vibration and that at 758 cm^{-1} is related to the C–H bending vibration. Consistent with the recorded FTIR spectra of similar MOF_S (Zhao et al. 2017), the FTIR spectrum presented

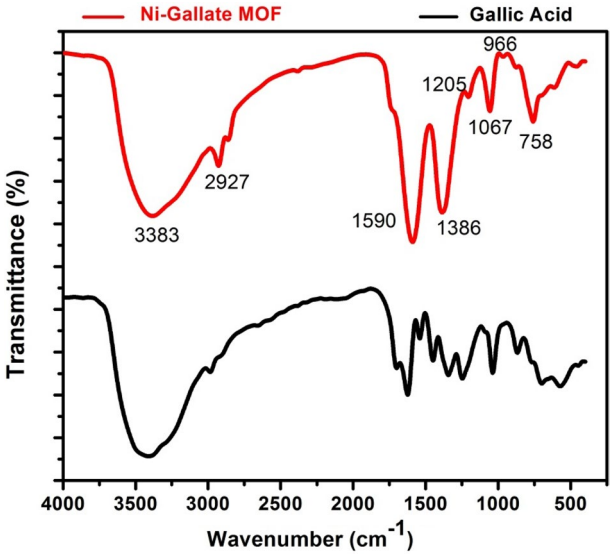

Fig. 2 FTIR spectra for the synthesized Ni-Gallate MOF (red) and Gallic acid powder (blue)

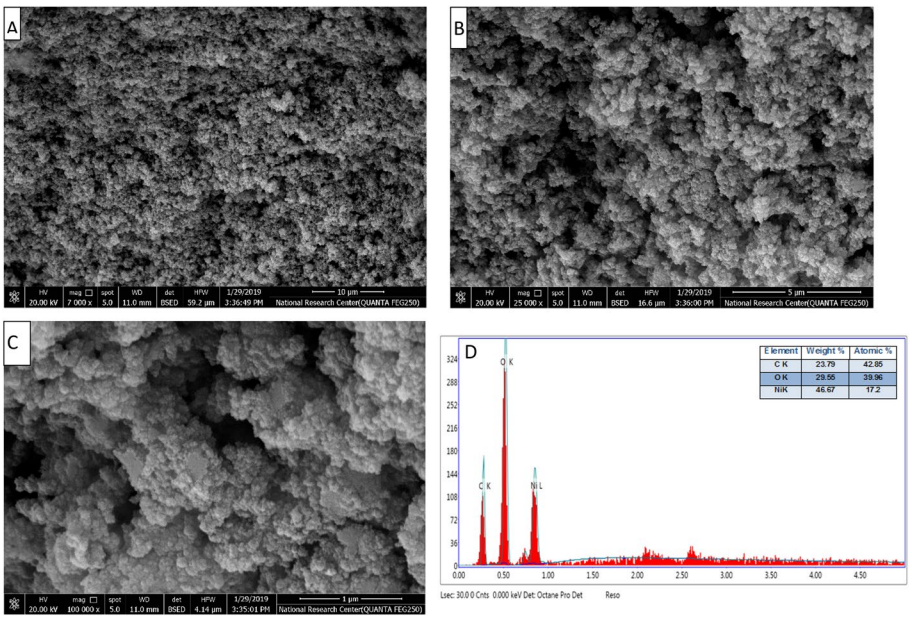

Fig. 3 SEM images of Ni-GA MOF nanoparticles (**A**, **B** and **C**). EDX analysis (**D**)

here for the synthesized nanostructure demonstrates the formation of a mesoporous Ni-GA MOF structures.

The morphology of the as-synthesized Ni-GA MOF is depicted in Fig. 3. The as-prepared Ni-GA MOF structures formed aggregates with distinct porosities, which are illustrated in Fig. 3c. These aggregates were based upon the assumption of the poor crystallinity of the prepared Ni-GA MOF, which in turn was as a result of the deprotonated Ni-GA MOF, in agreement with the result of XRD. Moreover, the EDX pattern shown in Fig. 3D demonstrates the presence of the elemental constituents of the Ni-GA MOF

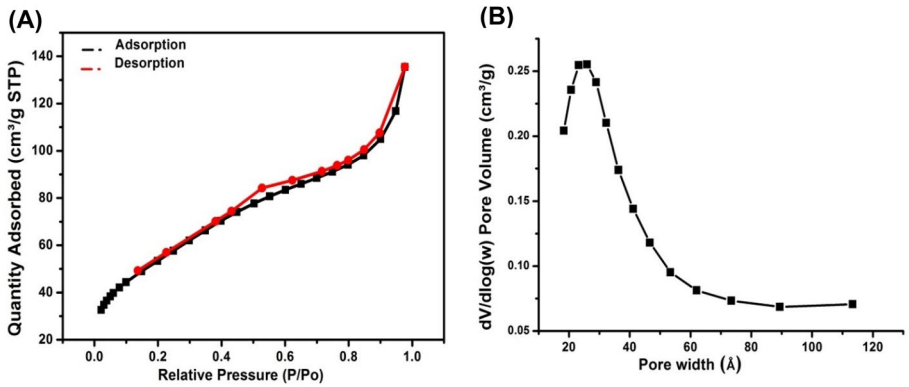

Fig. 4 Specific surface area analysis for the synthesized Ni–Gallate MOF, measured at 77 K. (**A**) N_2 adsorption/desorption isotherm curve. (**B**) Pore size distribution in Å

including Ni, O and C. The estimated quantity of Ni confirms the stoichiometric percentages of the elements in the structure; where the weight% ratio between Ni and C is approximately 2:1, which is in agreement with the ratios between the reactants (4 mmol $NiNO_3.6H_2O$: 2 mmol gallic acid monohydrate).

The surface area of the prepared Ni-gallate MOF was measured using N_2 gas adsorption, Fig. 4. The samples were degassed for 4 h at 80 °C under He gas flow. The adsorption/desorption isotherms indicate that the process is a type-IV with H3-type hysteresis loop, corresponding to materials with a mesoporous texture. The BET surface area at 77 K was 195 m^2g^{-1}. In addition, the total pore volume of the Ni-gallate MOF using the Barrett–Joyner–Halenda (BJH) adsorption method was 0.125 cm^3/g. The average pore size of the sample was found to equal 3.2 nm employing the BJH method to the N_2 desorption branch of the isotherm. Moreover, the average was distributed between 20 and 50 nm with an average value 30 nm, confirming the mesoporous characteristics of the Ni-gallate MOF structure, and with similar textural properties to the Cu-gallate MOF that was formerly reported (Banerjee et al. 2020).

Antibacterial assay

Figure 5 displays different plates of various strains of bacteria as Gram-positive (*Staphylococcus aureus, Streptococcus, Bacillus subtilis), and* Gram-negative (*E. coli* and *Pseudomonas aeruginosa)*. In addition, the figure shows the inhibition zone of each strain with variant concentrations of Ni-gallate MOF. The inhibition zone measured in millimeter (mm) by Agar diffusion method. Overall, the measured diameters were different from one species to another. And as such, Fig. 6A is a bar chart illustrates the calculated mean of the inhibition zone (mm) on the *Y*-axis at different concentrations of Ni-gallate-MOF (1000, 500, 250, 125, 62.5 µg/ml) versus diverse species of bacteria as mentioned above on *X*-axis. In total, the effect of Ni-gallate-MOF on the tested strains was uneven. First, regarding Gram-positive, the *S. aureus* was the highest responded followed by *St. coccus*, while the lowest one was *Bacillus subtilis*. Second, the response of *E. coli* Gram-negative was higher than that of *P. Aeruginosa*. Furthermore, the figure demonstrates that the inhibition zone was directly proportional to the concentration of Ni-gallate-MOF in all investigated species. The highest inhibition zone was about 37.5 mm and

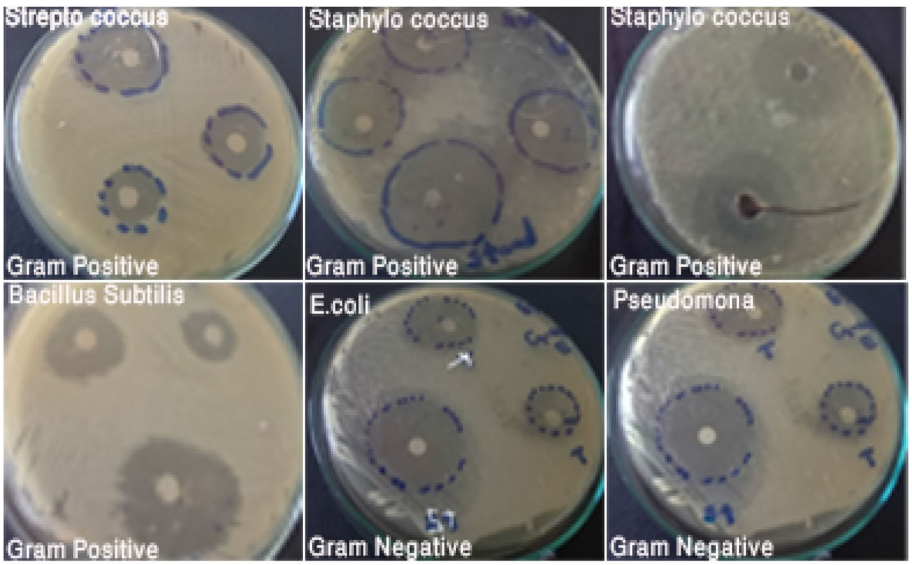

Fig. 5 Images showing the zone of inhibition (mm) Ni-Gallate MOF against different gram-positive and gram-negative bacterial strains

was measured in *S. aureus*, whereas the lowest one was approximately 17.5 mm and was recorded in *Bacillus subtilis*. It is worth mentioning that the tested Ni-gallate-MOF was compared with Draxxin for Gram-negative and tylvalosin from Gram-positive, the results had revealed that the effect of Ni-gallate-MOF and the compared standard drug was hardly the same in both Gram-negative and positive species. From this prospective point, the investigated Ni-gallate-MOF could act as an efficient alternative for bacterial resistance than the conventional antibiotics.

It should be noted that the MIC and MBC of the investigated Ni-gallate-MOF versus both Gram-positive and Gram-negative bacterial species, besides tested fungi such as *Aspergillus flocculosus* and *Aspergillus nigricans* are shown in Fig. 7. Actually, the figure reveals that the MIC value of the tested Ni-gallate-MOF was significantly distinct from one species to another, aside from, the recorded values of MBC and MIC are similar as in *Streptococcus pneumoniae*, *E. coli* and *Pseudomonas aeruginosa*; but, they were considerably different in *Staphylococcus aureus* as well in the tested fungi species. The figure exhibits the maximum value of MIC was slightly above 225 µg/ml and was recorded in *Pseudomonas aeruginosa*, whereas the minimum MIC value was about 35 µg/ml in *Staphylococcus aureus*. In relation to fungi, the MIC of *Aspergillus nigricans* was higher than that of *Aspergillus flocculosus*. Ordering of MIC value was the following: *Pseudomonas aeruginosa, E. coli, Aspergillus nigricans, Aspergillus flocculosus, Streptococcus pneumoniae, and Staphylococcus aureus.* On the other hand, the maximum value of MBC was recorded in *Aspergillus nigricans*, and the lowest one was in *Streptococcus pneumoniae.* The ordering of MBC was as follows: *Aspergillus flocculosus, Pseudomonas aeruginosa, E. coli, Staphylococcus aureus, and Streptococcus pneumoniae.* It is important to realize that the reason for this variation among strains is the divergence of the biological structures of these species. To sum up, the tested Ni-gallate-MOF has a potential effect on different strains of bacteria in a dose

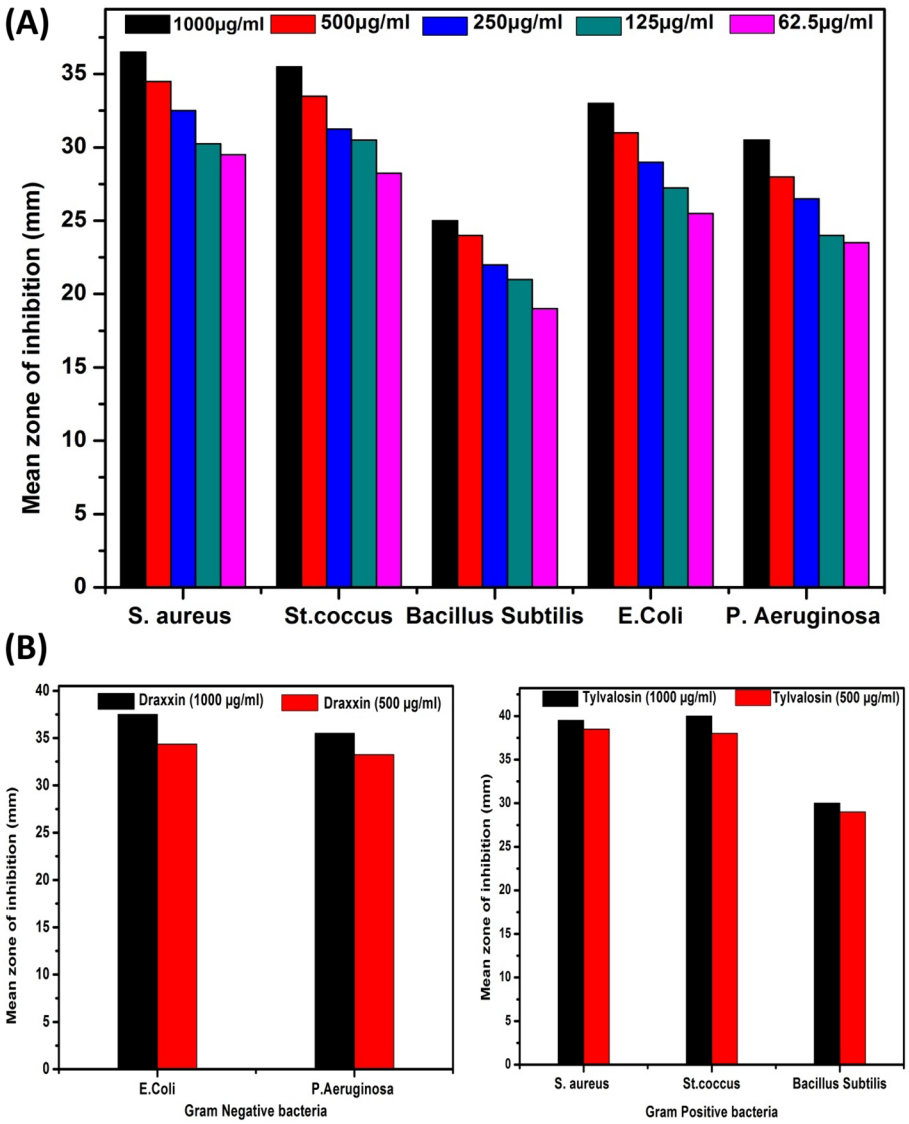

Fig. 6 (**A**) An illustration for the calculated mean of the inhibition zone (mm) at different concentrations of Ni-Gallate-MOF versus diverse species of bacteria. (**B**) displays the mean of inhibition zone against Standard antibiotics (Draxxin for Gram-negative and Tylvalosin for Gram-positive)

dependent manner, and in a distinct pattern, with higher activity against Gram positive than Gram negative, besides its antifungal efficiency.

Although, the actual mechanism or the interaction between metal organic framework structures and different pathogens is unknown, many hypotheses can be taken into account. In consensus with other studies (Lu et al. 2016; (Borges et al. 2013), the antibacterial activity of Ni-gallate-MOF might have been due to spontaneous release of free radicals such as ROS, inducing oxidative stress-mediated cell damage. To take into account, cell membrane damage might have been caused by the electrochemical mode of interaction between the Ni^{2+} ions with the phosphate group in the lipid layers, thereby disrupting cell membrane integrity and causing membrane leakage (Lu et al. 2016; (Borges et al. 2013). In much the same mechanism that proposed (Borges

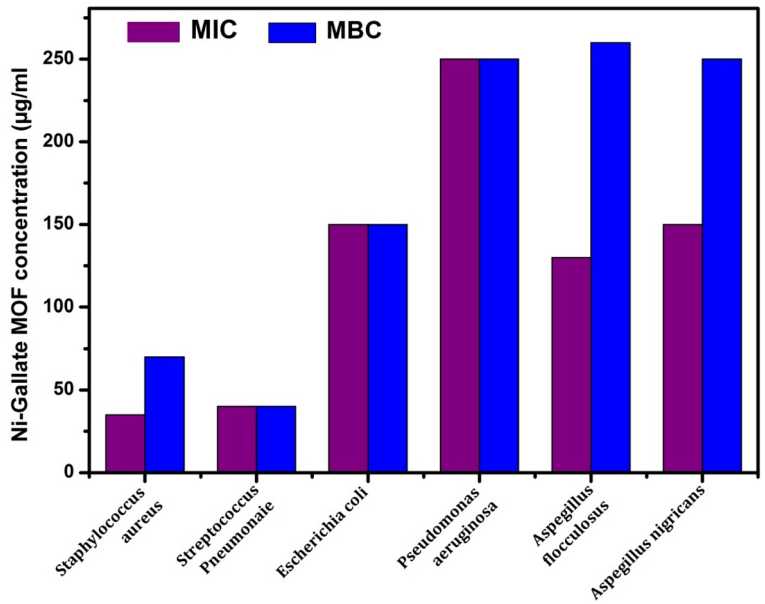

Fig. 7 Representation of the MIC and MBC values of Ni-Gallate MOF against gram-positive bacteria, gram-negative bacterial and fungi species

et al. 2013), in case of Gram-positive bacteria, the thin layer of peptidoglycan with abundant pores might have allowed the penetration of Ni-gallate-MOF into the cell resulting in membrane damage, cell content release and ultimately leading to cell death.

Similar to that of bacteria, the antifungal activity of Ni-gallate-MOF could be due to the electrostatic interaction between the phosphate group in the cell membrane and Ni^{2+}, penetration of Ni-gallate-MOF into the cell, gfollowed by binding of Ni^{2+} with the thiol group of protein leading to denaturation (Ferreira et al. 2011). Moreover, Ni-gallate-MOF might also have induced cellular death through ROS-mediated oxidative stress.

On the other hand, gallic acid might have a significant role; in particular, Jing et al. (2003) have demonstrated its antibacterial activity. Additionally, it was evidenced that gallic acid induced irreversible changes in cell membrane properties (charge, intra and extracellular permeability, and physicochemical properties) (Borges et al. 2013). The demonstrated mechanism of the gallic acid antimicrobial activity was through change in cell surface hydrophobicity, charge, induced PI uptake, and K^+ leakage with local rupture or pore formation in the cell membranes of Gram-negative and Gram-positive bacteria (Borges et al. 2013).

Anticancer measurements

The trypan blue dye exclusion test is utilized to measure the number of viable cells present in a cell suspension. It is based on the assumption that live cells possess intact cell membranes that block trypan blue dye, whereas trypan blue stain can move through entirely permeable membranes of the deceased cells, changing their color into blue, which is noticeable under optical microscopy. The treated RMS cell suspension with the

tested Ni-gallate MOF was infused with the trypan blue dye; it was visibly studied to check whether cells take up or prevent dye. The cytoplasm of the treated RMS cells was stained by blue color, while that of viable cells was clear. Comprehensive, the incubated cell lines with the medium containing the Ni-gallate MOF produced a considerable reduction in the number of viable cells contrast to the control group ($p < 0.05$).

The cytotoxicity of the investigated nanomaterials versus RMS was estimated by MTT assay. Figure 8a illustrates a statistical analysis bar chart of the MTT measurements. The chart shows, the cytotoxicity evaluation of Ni-gallate MOF, as well, a standard chemotherapy agent (doxorubicin) with serial dilutions (horizontal axis) versus RMS; the viability percent (vertical axis) of the treated cells was measured for each concentration. The data were reported as an average ± standard deviation. Overall, the viability of the treated RMS by doxorubicin reduced rapidly while those treated by the Ni-gallate MOF lessened consistently with no significant different in the viability percent at low

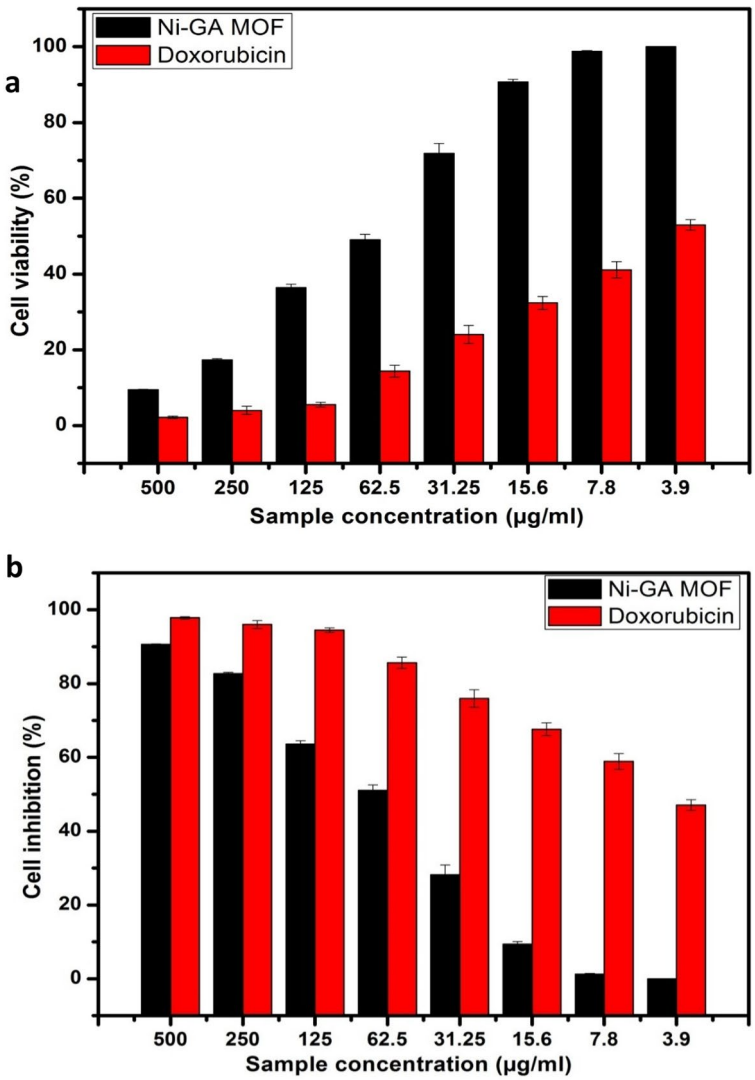

Fig. 8 The statistical analysis of the MTT assay, (**A**) the viability and (**B**) inhibitory percent of the RMS treated by Ni-Gallate MOF and the standard chemotherapy agent (Doxorubicin)

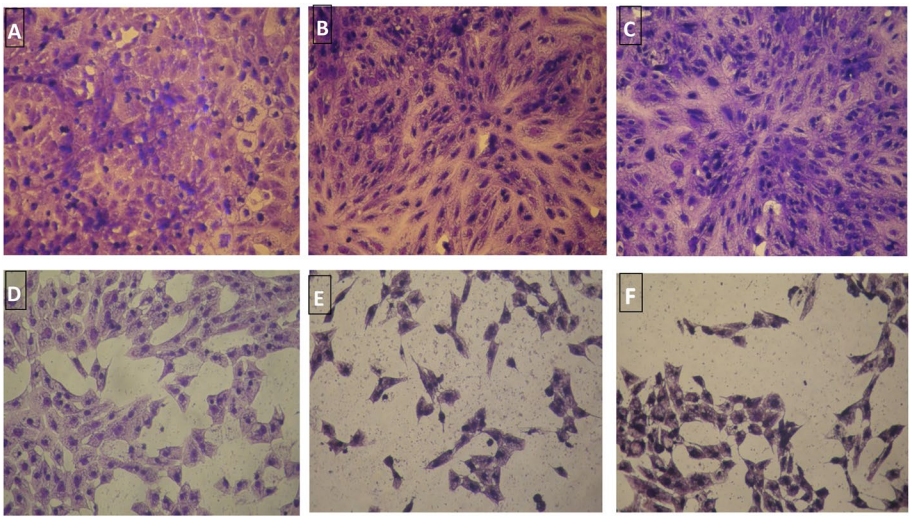

Fig. 9 Microscopy images showing the inhibitory activity against human muscle Rhabdomyosarcoma cell line carcinoma cells **A**) Untreated RD cells, **B**) Untreated Control, **C**) Treated with 15.6 µg MOF, **D**) Treated with 62.5 µg MOF, **E**) Treated with 125 µg MOF, **F**) Treated with 500 µg MOF

concentration and suddenly diminished at high concentration. As a whole, the viability percent of the treated RMS cells decreased with the increase of the concentration in both Ni-gallate MOF and doxorubicin. One can see that the lowest percent was at the concentration of (500 µg/ml); it was below 5% of doxorubicin and close to 10% of Ni-gallate MOF. On the other hand, Fig. 8b is a chart clarifies the inhibitory percent of the treated cell at the same concentrations. The IC_{50}% of the Ni-gallate MOF against RMS was 61.1 ± 1.7 µg/ml while that of doxorubicin was 4.8 ± 0.3 µg/ml.

Further, in the present investigation, the images of the inverted microscopy revealed distinct morphological variations in RMS cells treated with various concentrations of Ni-gallate MOF for 24 h comparing to the control. The adherent capacity of the RMS cells became poor and the shape became round as shown in Fig. 9. It is obviously clear that by extending the dose of Ni-gallate MOF, only a few cells kept in contact.

The mechanism of Ni-gallate MOF on the RMS is unknown, and investigating the mechanism of interaction between the RMS cell and the synthesized nanostructure requires a separate study. Furthermore, the results obtained here are consistent with the strong antioxidant, antiinflammatory, and anticancer properties of the gallic acid. In the presence of metal ions, it has pro-oxidant property in concentration dependent manner (Gressier et al. 1994). Moreover, it has been revealed that matrix metalloproteinase-2 (MMP-2) and MMP-9 proteolytic activities were inhibited via gallic acid (Lo et al. 2011). The prospective study investigates the apoptotic signaling pathway in RMS cells, which induced by Ni-gallate MOF.

Conclusion

In conclusion, we report the synthesis of a novel metal organic framework that exhibits an antimicrobial and anticancer activity against wide range of microbes and cancer cells. The natural antioxidant, gallic acid, has been used to synthesize a nickel-based metal organic framework (Ni-gallate MOF) using solvothermal methods. The Ni-gallate

MOF nanostructure was characterized using SEM, FTIR, XRD and BET surface area demonstrating that the structure shows zeolitic and MOF structural features (e.g., high microporosity). The as-synthesized Ni-gallate MOF nanostructures have shown high antibacterial activity against both Gram-positive and Gram-negative bacterial species, in addition to a wide spectrum antifungal activity. Furthermore, Ni-gallate MOF was found to inhibit the cancer cell growth in rhabdomyosarcoma (RMS), with an effectiveness quite significant, compared to the reference anticancer doxorubicin. Although, the mechanism of action for this anticancer and antimicrobial activity of the Ni-gallate MOF remains unknown, we speculate that incorporating a natural antioxidant (gallic acid) such as ligand in the synthesis of MOFs could produce reactive oxygen species (ROS) that are known to induce cell cytotoxicity on a wide range of cancer cells and antimicrobial activity. This opens real of opportunities for designing novel antimicrobial and anticancer materials.

Acknowledgements
Not applicable.

Author contributions
AAGE-S, EMD, SIE-D, Methodology, formal analysis, investigation, writing—review and editing AF, FIAE-E Validation, data curation, original draft preparation SIE, AF. All authors have read and agreed to the published version of the manuscript.

Funding
Open access funding provided by The Science, Technology & Innovation Funding Authority (STDF) in cooperation with The Egyptian Knowledge Bank (EKB). No funding available for this work.

Availability of data and materials
All data can be found in the article.

Declarations

Ethics approval and consent to participate
Not applicable.

Informed consent
Not applicable.

Competing of interests
All authors acknowledge that there are no competing interest regarding this work.

Received: 28 March 2023 Accepted: 2 May 2023
Published online: 09 June 2023

References

Badhani B, Sharma N, Kakkar R (2015) Gallic acid: a versatile antioxidant with promising therapeutic and industrial applications. RSC Adv 5(35):27540–27557
Banerjee S, Lollar CT, Xiao Z, Fang Y, Zhou H-C (2020) Biomedical integration of metal–organic frameworks. Trends Chem 2(5):467–479
Bernas T, Dobrucki J (2002) Mitochondrial and nonmitochondrial reduction of MTT: Interaction of MTT with TMRE, JC-1, and NAO mitochondrial fluorescent probes. Cytometry J Int Soc Anal Cytol 47(4):236–242
Boer JL, Mulrooney SB, Hausinger RP (2014) Nickel-dependent metalloenzymes. Arch Biochem Biophys 544:142–152
Borges A, Ferreira C, Saavedra MJ, Simões M (2013) Antibacterial activity and mode of action of ferulic and gallic acids against pathogenic bacteria. Microb drug Resist 19(4):256–265
Chambers HF, DeLeo FR (2009) Waves of resistance: *Staphylococcus aureus* in the antibiotic era. Nat Rev Microbiol 7(9):629–641
Chen B, Xiang S, Qian G (2010) Metal–organic frameworks with functional pores for recognition of small molecules. Acc Chem Res 43(8):1115–1124
Cooper L, Hidalgo T, Gorman M, Lozano-Fernández T, Simón-Vázquez R, Olivier C, Guillou N, Serre C, Martineau C, Taulelle F (2015) A biocompatible porous Mg-gallate metal–organic framework as an antioxidant carrier. Chem Commun 51(27):5848–5851
Czaja AU, Trukhan N, Müller U (2009) Industrial applications of metal–organic frameworks. Chem Soc Rev 38(5):1284–1293

DF SG, Rohwer LE, Rodriguez MA, Barnhart-Dailey MC, Butler KS, Luk TS, Timlin JA, Chapman KW (2017) Multifunctional, tunable metal–organic framework materials platform for bioimaging applications. ACS Appl Mater Interfaces 9(27):22268–22277
Dorman HD, Lantto TA, Raasmaja A, Hiltunen R (2011) Antioxidant, pro-oxidant and cytotoxic properties of parsley. Food Funct 2(6):328–337
Eckshtain-Levi M, Batty CJ, Lifshits LM, McCammitt B, Moore KM, Amouzougan EA, Stiepel RT, Duggan E, Ross TM, Bachelder EM (2022) Metal–organic coordination polymer for delivery of a subunit broadly acting influenza vaccine. ACS Appl Mater Interfaces 14(25):28548–28558
Feller RK, Cheetham AK (2006) Fe (III), mn (II), Co (II), and Ni (II) 3,4,5-trihydroxybenzoate (gallate) dihydrates; a new family of hybrid framework materials. Solid State Sci 8(9):1121–1125
Ferreira LS, Rodrigues MS, De Carvalho JCM, Lodi A, Finocchio E, Perego P, Converti A (2011) Adsorption of Ni2+, Zn2+ and Pb2+ onto dry biomass of Arthrospira (Spirulina) platensis and *Chlorella vulgaris*. I. single metal systems. Chem Eng J 173(2):326–333
Furukawa H, Cordova KE, O'Keeffe M, Yaghi OM (2013) The chemistry and applications of metal–organic frameworks. Science 341(6149):1230444
Gomha SM, Riyadh SM, Mahmmoud EA, Elaasser MM (2015) Synthesis and anticancer activity of arylazothiazoles and 1,3,4-thiadiazoles using chitosan-grafted-poly (4-vinylpyridine) as a novel copolymer basic catalyst. Chem Heterocycl Compd 51:1030–1038
Gressier B, Lebegue S, Brunet C, Luyckx M, Dine T, Cazin M, Cazin J (1994) Pro-oxidant properties of methotrexate: evaluation and prevention by an anti-oxidant drug. Pharmazie 49(9):679–681
Horcajada P, Chalati T, Serre C, Gillet B, Sebrie C, Baati T, Eubank JF, Heurtaux D, Clayette P, Kreuz C (2010) Porous metal–organic-framework nanoscale carriers as a potential platform for drug delivery and imaging. Nat Mater 9(2):172–178
Jiao Y, Pei J, Chen D, Yan C, Hu Y, Zhang Q, Chen G (2017) Mixed-metallic MOF based electrode materials for high performance hybrid supercapacitors. J Mater Chem A 5(3):1094–1102
Jing W, Demcoe AR, Vogel HJ (2003) Conformation of a bactericidal domain of puroindoline a: structure and mechanism of action of a 13-residue antimicrobial peptide. J Bacteriol 185(16):4938–4947
Kaur N, Tiwari P, Kapoor KS, Saini AK, Sharma V, Mobin SM (2020) Metal–organic framework based antibiotic release and antimicrobial response: an overview. CrystEngComm 22(44):7513–7527
Kitagawa S, Kitaura R, Noro, Si (2004) Functional porous coordination polymers. Angew Chem Int Ed 43(18):2334–2375
Kumar P, Deep A, Kim K-H (2015) Metal organic frameworks for sensing applications. TRAC Trends Anal Chem 73:39–53
Lawson HD, Walton SP, Chan C (2021) Metal–organic frameworks for drug delivery: a design perspective. ACS Appl Mater Interfaces 13(6):7004–7020
Liu D, Lu K, Poon C, Lin W (2014) Metal–organic frameworks as sensory materials and imaging agents. Inorg Chem 53(4):1916–1924
Lo C, Lai T-Y, Yang J-S, Yang J-H, Ma Y-S, Weng S-W, Lin H-Y, Chen H-Y, Lin J-G, Chung J-G (2011) Gallic acid inhibits the migration and invasion of A375. S2 human melanoma cells through the inhibition of matrix metalloproteinase-2 and ras. Melanoma Res 21(4):267–273
Lu J, Wang Z, Ren M, Huang G, Fang B, Bu X, Liu Y, Guan S (2016) Antibacterial effect of gallic acid against *Aeromonas hydrophila* and *Aeromonas sobria* through damaging membrane integrity. Curr Pharm Biotechnol 17(13):1153–1158
Maranescu B, Visa A (2022) Applications of metal-organic frameworks as drug delivery systems. Int J Mol Sci 23(8):4458
Masoud MS, Hagagg SS, Ali AE, Nasr NM (2012) Synthesis and spectroscopic characterization of gallic acid and some of its azo complexes. J Mol Struct 1014:17–25
McKinlay AC, Morris RE, Horcajada P, Férey G, Gref R, Couvreur P, Serre C (2010) BioMOFs: metal–organic frameworks for biological and medical applications. Angew Chem Int Ed 49(36):6260–6266
Mu X, Yan C, Tian Q, Lin J, Yang S (2017) BSA-assisted synthesis of ultrasmall gallic acid–Fe (III) coordination polymer nanoparticles for cancer theranostics. Int J Nanomed 12:7207
Park SH (2014) Third-generation cephalosporin resistance in gram-negative bacteria in the community: a growing public health concern. Korean J Intern Med 29(1):27
Ponce A, Brostoff LB, Gibbons SK, Zavalij P, Viragh C, Hooper J, Alnemrat S, Gaskell KJ, Eichhorn B (2016) Elucidation of the Fe (III) gallate structure in historical iron gall ink. Anal Chem 88(10):5152–5158
Ren Y, Deng H, Shen W, Gao Z (2013) A highly sensitive and selective electrochemical biosensor for direct detection of microRNAs in serum. Anal Chem 85(9):4784–4789
Sourani Z, Pourgheysari B, Beshkar P, Shirzad H, Shirzad M (2016) Gallic acid inhibits proliferation and induces apoptosis in lymphoblastic leukemia cell line (C121). Iran J Med Sci 41(6):525
Tanabe KK, Cohen SM (2011) Postsynthetic modification of metal–organic frameworks—a progress report. Chem Soc Rev 40(2):498–519
Wang Q, de Oliveira EF, Alborzi S, Bastarrachea LJ, Tikekar RV (2017) On mechanism behind UV-A light enhanced antibacterial activity of gallic acid and propyl gallate against *Escherichia coli* O157: H7. Sci Rep 7(1):8325
Wu MX, Yang YW (2017) Metal–organic framework (MOF)-based drug/cargo delivery and cancer therapy. Adv Mater 29(23):1606134
Wyszogrodzka G, Marszałek B, Gil B, Dorożyński P (2016) Metal–organic frameworks: mechanisms of antibacterial action and potential applications. Drug Discov Today 21(6):1009–1018
Yan L, Gopal A, Kashif S, Hazelton P, Lan M, Zhang W, Chen X (2022) Metal organic frameworks for antibacterial applications. Chem Eng J 134975.
Yaghi OM, O'Keeffe M, Ockwig NW, Chae HK, Eddaoudi M, Kim J (2003) Reticular synthesis and the design of new materials. Nature 423(6941):705–714
Zhao X, Tan Y, Wu F, Niu H, Tang Z, Cai Y, Giesy JP (2016) Cu/Cu2O/CuO loaded on the carbon layer derived from novel precursors with amazing catalytic performance. Sci Total Environ 571:380–387
Zhao Q, Yan Z, Chen C, Chen J (2017) Spinels: controlled preparation, oxygen reduction/evolution reaction application, and beyond. Chem Rev 117(15):10121–10211

Zhou D-N, Yang Q-Q, Li Z-L, Pan Z-Y, Deng Y-F (2015) Head and neck rhabdomyosarcoma: follow-up results of four cases and review of the literature. Int J Clin Exp Pathol 8(5):4277

Publisher's Note